Exploring the Physical Basis of Solar Cycle Predictions: Flux Transport Dynamics and Persistence of Memory in Advection versus Diffusion Dominated Solar Convection Zones

Anthony R. Yeates

School of Mathematics and Statistics, University of St Andrews, St Andrews, KY16 9SS, UK

anthony@mcs.st-and.ac.uk

Dibyendu Nandy

Department of Physics, Montana State University, Bozeman, MT 59717, USA

nandi@mithra.physics.montana.edu

and

Duncan H. Mackay

School of Mathematics and Statistics, University of St Andrews, St Andrews, KY16 9SS, UK

duncan@mcs.st-and.ac.uk

ABSTRACT

The predictability, or lack thereof, of the solar cycle is governed by numerous separate physical processes that act in unison in the interior of the Sun. Magnetic flux transport and the finite time delay it introduces, specifically in the so-called Babcock-Leighton models of the solar cycle with spatially segregated source regions for the α and Ω-effects, play a crucial rule in this predictability. Through dynamo simulations with such a model, we study the physical basis of solar cycle predictions by examining two contrasting regimes, one dominated by diffusive magnetic flux transport in the solar convection zone, the other dominated by advective flux transport by meridional circulation. Our analysis shows that diffusion plays an important role in flux transport, even when the solar cycle period is governed by the meridional flow speed. We further examine the persistence of memory of past cycles in the advection and diffusion dominated regimes through stochastically forced dynamo simulations. We find that

in the advection-dominated regime, this memory persists for up to three cycles, whereas in the diffusion-dominated regime, this memory persists for mainly one cycle. This indicates that solar cycle predictions based on these two different regimes would have to rely on fundamentally different inputs – which may be the cause of conflicting predictions. Our simulations also show that the observed solar cycle amplitude-period relationship arises more naturally in the diffusion dominated regime, thereby supporting those dynamo models in which diffusive flux transport plays a dominant role in the solar convection zone.

Subject headings: Sun: activity — Sun: interior — Sun: magnetic fields

1. Introduction

Direct observations of sunspot numbers over 400 years, as well as proxy data for much longer timescales (Beer 2000), show that both the amplitude and the duration of the solar magnetic cycle vary from one cycle to the next. The importance of this phenomenon lies in the contribution of varying levels of solar activity to long-term climate change, and to short-term space weather (Nandy & Martens 2007). While there is now a concensus that the Sun's magnetic field is generated by a hydromagnetic dynamo (Ossendrijver 2003; Charbonneau 2005), the origin of fluctuations in the basic cycle is yet to be conclusively determined. Several different mechanisms have been proposed, including nonlinear effects (Tobias 1997; Beer et al. 1998; Knobloch et al. 1998; Küker et al. 1999; Wilmot-Smith et al. 2005), stochastic forcing (Choudhuri 1992; Hoyng 1993; Ossendrijver et al. 1996; Charbonneau & Dikpati 2000; Mininni & Gómez 2002), and time-delay dynamics (Yoshimura 1978; Durney 2000; Charbonneau et al. 2005; Wilmot-Smith et al. 2006). A coupled, equally important, but ill-understood issue is how the memory of these fluctuations, whatever may be its origin, carries over from one cycle to another mediated via flux transport processes within the solar convection zone (SCZ). A unified understanding of all these disparate processes lays the physical foundation for the predictability (or lack-thereof) of future solar activity. These considerations motivate the current study.

The main flux transport processes in the SCZ involve magnetic buoyancy (timescale on the order of months), meridional circulation, diffusion and downward flux-pumping (timescales relatively larger). Because magnetic buoyancy, i.e., the buoyant rise of magnetic flux tubes, acts on timescales much shorter than the solar cycle timescale, the fluctuations that it produces are also short-lived in comparison. Our focus here is on longer-term fluctuations, on the order of the solar cycle period, that may lead to predictive capabilities.

Through an analysis of observational data, Hathaway et al. (2003) have shown that the solar cycle amplitude and duration are correlated with the equatorward drift velocity of the sunspot belts during the cycle. They associate this drift velocity with the deep meridional counterflow that must exist to balance the poleward flows that are observed at the surface (Hathaway 1996, 2005; Miesch 2005). The results show a significant negative correlation between the drift velocity and the cycle duration, so that the drift is faster in shorter cycles, consistent with the interpretation of meridional circulation as the timekeeper of the solar cycle (Nandy 2004; but see also Schüssler & Schmitt 2004). In addition Hathaway et al. (2003) identified positive correlations between the drift velocity of cycle n and the amplitudes of both cycles n and $n + 2$. While the two-cycle time lag was a new result, the positive correlation between circulation speed and amplitude of the same cycle is supported by several earlier studies. In their surface flux transport model, Wang et al. (2002) needed a varying meridional flow, faster in higher-amplitude cycles, to sustain regular reversals in the Sun's polar field. They cited observational evidence from polar faculae counts (Sheeley 1991), which peaked early for two of the stronger cycles, coinciding with poleward surges of magnetic flux. Furthermore, observations show a statistically-significant negative correlation between peak sunspot number and the duration of cycles 1 to 22 (Figure 1c of Charbonneau & Dikpati 2000; see also Solanki et al. 2002). Such a negative correlation between cycle amplitude and duration is also found in the models of Hoyng (1993) and Charbonneau & Dikpati (2000). Taken with the inverse relation between cycle duration and circulation speed, this is again suggestive of a positive correlation between circulation speed and cycle amplitude.

Meridional circulation plays an important role in a certain class of theoretical solar cycle models often referred to as "flux-transport", "advection-dominated," or "circulation-dominated" dynamo models (see, e.g., the review by Nandy 2004). Such models have gained popularity in recent years owing to their success in reproducing various observed features of the solar cycle (Choudhuri et al. 1995; Durney 1995; Dikpati & Charbonneau 1999; Küker et al. 2001; Bonanno et al. 2002; Nandy & Choudhuri 2001, 2002; Chatterjee et al. 2004). In these models, a single-cell meridional circulation in each hemisphere (which is observed at the solar surface) is invoked to transport poloidal field, first poleward at near-surface layers and then down to the tachocline where toroidal field is generated. Subsequently, the return flow in the circulation advects this toroidal field belt equatorward through a region at the base of the SCZ which is characterized by low diffusivity. From this deep toroidal field belt, destabilized flux tubes rise to the surface due to magnetic buoyancy, producing sunspots (Parker 1955). We may point out here that the name "flux-transport dynamo" is somewhat inappropriate to classify a circulation or advection-dominated dynamo (where the diffusion timescale is much larger than the circulation timescale throughout the dynamo domain). Our results indicate that diffusive flux-transport in the SCZ could play a dominant role in

dynamos even when the cycle period is governed by meridional circulation speed, pointing out that flux-transport is a shared process. So, henceforth, by "flux-transport" dynamo, we imply a dynamo where the transport of magnetic field is shared by magnetic buoyancy, meridional circulation, and diffusion.

Flux-transport dynamos offer the possibility of prediction because of their inherent memory. This arises specifically when the dynamo source regions for poloidal field production (the traditional α-effect) and toroidal field generation (the Ω-effect) are spatially segregated. A brief discussion on important timescales (we identify three significant ones) in the dynamo process is merited here. The first is governed by the buoyant rise of toroidal flux tubes from the Ω-effect layer to the α-effect layer to generate the poloidal field; since this is a fast process on the order of months, no significant memory is introduced here. The second involves the transport of poloidal field back into the Ω-effect layer (either by circulation or diffusion). This could be a slow process where significant memory is introduced which is dominated by the fastest of the competing processes (advection versus diffusion). The third timescale relates to the slow equatorward transport of the toroidal field belt through the base of the SCZ, which sets the period of the sunspot cycle. In this class of dynamo models, with meridional circulation and low diffusivities in the tachocline (at the base of the SCZ), the third timescale is almost invariably determined by the circulation speed. It is the second timescale above, with competing effects of diffusive flux transport and advective flux transport, that becomes important in the context of the persistence of memory. In the advection-dominated, stochastically fluctuating model of Charbonneau & Dikpati (2000), this second timescale (governed by advection of poloidal field due to meridional circulation) was about 17 years, so that the polar field at the end of cycle n correlated strongest with the toroidal field of cycle $n + 2$ rather than that of cycle $n + 1$. The length of memory of any particular flux-transport dynamo model is unfortunately dependent on the internal meridional flow profile, and on other chosen properties of the convection zone which are not yet well-determined observationally. A particular problem is the strength of diffusivity in the convection zone, which strongly affects the mode of operation of the dynamo.

Even if one assumes that these flux-transport dynamos capture enough of the realistic physics of the SCZ to make predictions of future solar activity, these predictions are critically dependent on the relative role of diffusion and advection in the SCZ. Dikpati & Gilman (2006), in their highly *advection-dominated* model, show that bands of latitudinal field from three previous cycles remain "lined up in the meridional circulation conveyor belt". They suggest that poloidal fields from cycles $n-3$, $n-2$, and $n-1$ combine to produce the toroidal field of cycle n. Based on an assumed proxy for the solar poloidal fields (sunspot area), this leads them to predict that Cycle 24 will be about 50% stronger than Cycle 23 (Dikpati et al. 2006). In stark contrast, Choudhuri et al. (2007), using a flux-transport dynamo model

with *diffusion-dominated* SCZ, and using as inputs the observed strength of the solar dipole moment (as a proxy for the poloidal field), predict that Cycle 24 will be about 35% *weaker* than Cycle 23. Choudhuri et al. (2007) argue that the main contribution to the toroidal field of cycle n, comes only from the polar field of cycle $n-1$ (see also Jiang et al. 2007 for further details of this model).

The conflicting predictions from these two solar dynamo models presumably result from the difference in the memory (i.e., survival) of past cycle fields in these models and could be to some extent influenced by the different inputs they use as proxies for the solar poloidal field. We also hypothesize that stronger diffusion in the Choudhuri et al. (2007) model destroys polar field faster, and that flux transport by diffusion across the SCZ in this model short-circuits the meridional circulation conveyor belt, thereby shortening the memory of previous cycles. We perform a detailed analysis to test these ideas. To begin with, we consider a wider parameter space in the present paper, where we study the effect of varying meridional circulation speed and SCZ diffusivity on the amplitude and period of the solar cycle. In these simulations, we keep all other parameters the same, allowing a direct comparison between advection-dominated and diffusion-dominated SCZ regimes – which has previously been clouded by other differences between models. Then we introduce stochastic fluctuations in the model α-effect to self-consistently generate cycle-amplitude variations – as a completely theoretical construct towards studying cycle-to-cycle variations, in contrast to using diverse observed proxies for time-varying poloidal fields. Subsequently, we perform a comparative analysis of the persistence of memory in this stochastically forced dynamo model in both the advective and diffusive flux-transport dominated regimes. Therefore, in spirit, this paper deals with the underlying physics of solar cycle predictability, and is not concerned with making a prediction itself. The layout of this paper is as follows. The main features of the model are summarised in Section 2, and the results of the parameter-space study are presented in Section 3. These results are interpreted in Section 4. In Section 5 we analyze the persistence of memory in the advection versus diffusion dominated regimes. We conclude in Section 6 with a discussion on the relevance of this work in the context of developing predictive capabilities for the solar activity cycle.

2. The Model

We use the solar dynamo code *Surya*, which has been studied extensively in different contexts (e.g. Nandy & Choudhuri 2002, Chatterjee et al. 2004, Chatterjee & Choudhuri 2006), and is made available to the public on request. The major ingredients of the code include an analytic fit to the helioseismically-determined differential rotation profile, a single-

cell meridional circulation in the SCZ, different diffusivities for the toroidal and poloidal fields, a buoyancy algorithm to model radial transport of magnetic flux, and a Babcock-Leighton (BL; Babcock 1961, Leighton 1969) type α-effect localized near the surface layer (signifying the generation of poloidal field due to the evolution of tilted bipolar sunspot pairs under surface flux transport). The code solves the kinematic mean-field dynamo equations for an axisymmetric magnetic field, which may be expressed in spherical coordinates (r, θ, ϕ) as

$$\mathbf{B} = B(r,\theta)\mathbf{e}_\phi + \mathbf{B}_\mathrm{p}, \tag{1}$$

where $B(r,\theta)$ and $\mathbf{B}_\mathrm{p} = \nabla \times [A(r,\theta)\mathbf{e}_\phi]$ correspond to the toroidal and poloidal components respectively. The mean-field MHD induction equation (see e.g. Moffatt 1978) then leads to the following standard equations for the α-Ω dynamo problem:

$$\frac{\partial A}{\partial t} + \frac{1}{s}\left(\mathbf{v}\cdot\nabla\right)(sA) = \eta_p\left(\nabla^2 - \frac{1}{s^2}\right)A + \alpha B, \tag{2}$$

$$\frac{\partial B}{\partial t} + \frac{1}{r}\left(\frac{\partial}{\partial r}\left(rv_r B\right) + \frac{\partial}{\partial\theta}\left(v_\theta B\right)\right) = \eta_t\left(\nabla^2 - \frac{1}{s^2}\right)B + s\left(\mathbf{B}_\mathrm{p}\cdot\nabla\right)\Omega + \frac{1}{r}\frac{d\eta_t}{dr}\frac{\partial}{\partial r}\left(rB\right). \tag{3}$$

Here $s = r\sin\theta$, and we specify the meridional flow $\mathbf{v}$, the internal angular velocity Ω, the diffusivities η_p and η_t, and the coefficient α for the BL α-effect which describes the generation of poloidal field at the solar surface from the decay of bipolar sunspots. Note that although for modelling purposes the BL α-effect is mathematically similar to the traditional mean-field α-effect due to small-scale helical turbulence, the former is fundamentally different. The BL α-effect acts on much larger spatial (on the order of active regions or greater) and temporal (surface flux transport) scales, and is quenched at much stronger field strengths (10^5G). The profiles of Ω and α were described in Chatterjee et al. (2004) and will not be repeated here. We will, however, describe the meridional circulation and diffusivity profiles in more detail.

2.1. Meridional Circulation

The meridional circulation is defined in terms of a streamfunction $\psi(r,\theta)$, giving the velocity by

$$\rho\mathbf{v} = \nabla\times\left[\psi(r,\theta)\mathbf{e}_\phi\right], \tag{4}$$

where we assume the density stratification

$$\rho = C\left(R_\odot/r - 0.95\right)^{3/2}. \tag{5}$$

The streamfunction is given by

$$\psi r \sin\theta = \psi_0 \, (r - R_p) \sin\left(\frac{\pi(r - R_p)}{R_\odot - R_p}\right) \times \left\{1 - \mathrm{e}^{-\beta_1 \theta^\epsilon}\right\} \left\{1 - \mathrm{e}^{\beta_2(\theta - \pi/2)}\right\} \mathrm{e}^{-((r-r_0)/\Gamma)^2}, \quad (6)$$

where $\beta_1 = 1.5 \times 10^{-8}\,\mathrm{m}^{-1}$, $\beta_2 = 1.8 \times 10^{-8}\,\mathrm{m}^{-1}$, $\epsilon = 2.0000001$, $\Gamma = 3.47 \times 10^8\,\mathrm{m}$, and $r_0 = (R_\odot - R_b)/4$. Here $R_\odot = 6.96 \times 10^8\,\mathrm{m}$ is the radius of the Sun, $R_b = 0.55R_\odot$ is the bottom of the simulation domain, and $R_p = 0.61R_\odot$ is the penetration depth of the meridional circulation. We combine the arbitrary constants C and ψ_0 in the parameter $v_0 = -\psi_0/(0.95C)$ which gives, approximately, the flow speed near the surface at mid-latitudes. It is this parameter v_0 which we vary to change the circulation speed in this study.

The circulation profile is illustrated in Figure 1 for $v_0 = 25\,\mathrm{m\,s^{-1}}$. The dots are plotted at yearly intervals for particles moving along the streamlines shown.

2.2. Diffusion

We use different diffusivities for the toroidal and poloidal fields, defined as follows:

$$\eta_t(r) = \eta_{RZ} + \frac{\eta_1 - \eta_{RZ}}{2}\left[1 + \mathrm{erf}\left(\frac{r - r'_{BCZ}}{d_t}\right)\right] + \frac{\eta_0 - \eta_1}{2}\left[1 + \mathrm{erf}\left(\frac{r - r_{TCZ}}{d_t}\right)\right], \quad (7)$$

$$\eta_p(r) = \eta_{RZ} + \frac{\eta_2 - \eta_{RZ}}{2}\left[1 + \mathrm{erf}\left(\frac{r - r_{BCZ}}{d_t}\right)\right] + \frac{\eta_0 - \eta_2}{2}\left[1 + \mathrm{erf}\left(\frac{r - r_{TCZ}}{d_t}\right)\right]. \quad (8)$$

Here $d_t = 0.025R_\odot$, $r_{BCZ} = 0.7R_\odot$, $r'_{BCZ} = 0.72R_\odot$, and $r_{TCZ} = 0.975R_\odot$. In the radiative core we choose a low diffusivity, namely $\eta_{RZ} = 2.2 \times 10^8\,\mathrm{cm^2\,s^{-1}}$, representing molecular diffusivity only since there is no turbulent convection. We always choose $\eta_1 < \eta_2$ so that the toroidal field diffusivity η_t in the convection zone is lower than the poloidal field diffusivity η_p. This is to model the suppression of turbulent diffusivity by strong magnetic fields, as toroidal field tends to be strong and concentrated in localised flux tubes and therefore subject to less diffusion (Choudhuri 2003), whereas poloidal field is weaker and subject to more diffusion. At the surface both diffusivities increase to a high value (of the order of $10^{12}\,\mathrm{cm^2\,s^{-1}}$), in line with surface flux transport models and observational estimates. Typical profiles are illustrated in Figure 2.

2.3. Numerical Domain and Boundary Conditions

We solve Equations (2) and (3) in a meridional plane $0.55R_\odot < r < R_\odot$, $0 < \theta < \pi/2$, representing the Northern hemisphere. This is divided into a spherical grid of 128 by 128 cells, uniformly spaced in r and θ. We use the same boundary conditions as Chatterjee et al. (2004), except that we consider only the Northern hemisphere and set $B = 0$ and $\partial A/\partial\theta = 0$ at the equator ($\theta = \pi/2$), thereby forcing the solution to have dipolar parity.

2.4. Example Solutions

Example solutions for two different runs are shown in time-latitude plots in Figures 3(a) and (b), where the black lines denote contours of toroidal field strength at the base of the convection zone ($r = 0.71R_\odot$). This corresponds to the solar butterfly diagram, with the strongest field located at the active latitudes and migrating equatorward during each cycle. The background shading shows the strength of the radial field at the solar surface ($r = R_\odot$), which peaks at the pole several years after the toroidal field maxima (of the same sign) at low latitudes. The two solutions in Figure 3 characterize the diffusion-dominated SCZ (Figure 3a) and advection-dominated SCZ (Figure 3b) regimes of the dynamo. In Figure 3(b) the toroidal field shows a poleward branch at high latitude which is absent in Figure 3(a), and also a stronger radial polar field at the surface. The cause of these differences between the two regimes will become clear in Section 4.

3. Results

We have carried out a parameter-space study to investigate how the cycle duration and amplitude in our model depend on the speed of meridional circulation and on the diffusivity in the convection zone. In each run of the code the parameters are held constant in time, but they are varied between different runs. Specifically, we vary the parameter v_0, which gives the maximum circulation speed, and also η_2, which affects the diffusive decay and transport of the *poloidal* field in the convection zone, but not the toroidal field. In all runs we keep a surface diffusivity of $\eta_0 = 2.0 \times 10^{12}\,\mathrm{cm^2\,s^{-1}}$, and a toroidal field diffusivity of $\eta_1 = 0.04 \times 10^{12}\,\mathrm{cm^2\,s^{-1}}$ in the convection zone. These choices approximate the fact that turbulent diffusion is expected to be more efficient in the decay and dispersal of the weaker poloidal field, but less so for the stronger toroidal field; the latter suppresses the convective motions that give rise to turbulent diffusivity in the first place. The α-effect coefficient is not varied, but is set to $\alpha_0 = 30\,\mathrm{m\,s^{-1}}$ for each run. This particular value was chosen to

ensure that periodic solutions could be obtained for a wide range of the parameters v_0 and η_2. Each run was started from an arbitrary initial state, and then evolved until initial transients had disappeared, leaving a steady periodic dynamo solution. Such a periodic solution was found to exist only within a certain range of v_0 for each value of η_2. The cycle duration and amplitude were then measured from the periodic solutions, in the cases where such a solution was found.

We define the cycle duration and amplitude by considering the time evolution of the toroidal magnetic flux $\Phi_{\rm tor}$ in a certain region around the base of the convection zone. Specifically, the toroidal field $B(r,\theta)$ is integrated at each time step over a region $r = 0.677R_\odot$ to $0.726R_\odot$, $\theta = 45^\circ$ to 80° (i.e., over the tachocline and latitudes 45° to 10°). This magnetic flux $\Phi_{\rm tor}$ should be proportional to the active region magnetic flux at the solar surface, under the assumption that more toroidal flux at the base of the convection zone leads to more buoyant eruptions. In a steady dynamo solution the flux $\Phi_{\rm tor}$ varies in strictly periodic manner, with its maximum amplitude giving the "cycle amplitude". We define the "cycle duration" to be the interval between successive peaks of $|\Phi_{\rm tor}|$ (half of the full dynamo period). This is therefore equivalent to the standard definition of the 11-year solar activity cycle, but of course the simulated periods are different.

The resulting cycle duration and cycle amplitude are plotted as functions of the circulation speed v_0 in Figures 4 and 5 respectively. In these figures each curve corresponds to a different value of the diffusivity η_2. The range of speeds covered by each curve indicates the range for which the code relaxed to a steady periodic dynamo solution, up to a maximum of $v_0 = 38\,{\rm m\,s^{-1}}$. In Figure 6 the cycle amplitude is plotted as a function of η_2, and in this case each curve corresponds to a different circulation speed v_0.

3.1. Dependence of Cycle Period on Meridional Circulation and Diffusion

Figure 4 shows a clear inverse dependence of the cycle duration on the meridional circulation speed v_0, with faster circulation leading to shorter cycles. A least-squares fit for the curve with $\eta_2 = 0.5 \times 10^{12}\,{\rm cm^2\,s^{-1}}$ gives the dependence of the cycle period on meridional flow speed

$$T = 217.716\, v_0^{-0.885}, \tag{9}$$

where T is in years and v_0 is in metres per second. This agrees with the $T \sim v_0^{-0.89}$ found by Dikpati & Charbonneau (1999), and this inverse relation is a well-established result for Babcock-Leighton dynamo models. In these models the circulation, and specifically the equatorward counterflow at the bottom of the convection zone, is the primary determinant of the cycle period (Nandy 2004).

The cycle duration is only weakly dependent on the diffusivity η_2. A power-law fit for the curve with $\eta_2 = 2.0 \times 10^{12}\,\mathrm{cm^2\,s^{-1}}$ gives $T = 150.745\,v_0^{-0.756}$ years. The lower power of v_0 here indicates that for higher-diffusivity solutions the cycle duration is slightly less dependent on circulation speed, presumably because flux transport by diffusive dispersal starts becoming important. Also, it is evident from Figure 4 that, at lower circulation speeds, there is a maximum diffusivity for which a periodic solution can exist. If there is too much diffusion at a low circulation speed, then the poloidal field will decay too much during its transport from high to low latitudes, thus generating insufficient toroidal field to sustain a periodic dynamo process. The essential difference between advective and diffusive flux transport is that the latter also reduces field strength during transport, due to diffusive decay.

3.2. Dependence of Cycle Amplitude on Meridional Circulation and Diffusion

Now we turn to the dependence of cycle amplitude on the speed of meridional circulation. This is shown in Figure 5, where each curve corresponds to a different diffusivity η_2 according to the legend. Rather than being monotonic, the cycle amplitude first increases with v_0 for low v_0 and then decreases with v_0 for large v_0, with a turnover at some value of v_0 in between. The location of this turnover shifts to higher speeds as the diffusivity is increased.

The dependence of cycle amplitude on diffusivity at any given circulation speed is not entirely clear on Figure 5, but is evident in Figure 6, where cycle amplitude is plotted against diffusivity η_2. In this figure each curve corresponds to a different value of the circulation speed v_0. We see a similar behavior in that the cycle amplitude first increases with η_2 for low η_2 and then decreases with η_2 for high η_2, with a turnover in between. If the circulation speed is increased, then the value of η_2 corresponding to this turnover also increases.

The behaviour of the cycle amplitude in our model, as illustrated in Figures 5 and 6, is more complex than expected *a priori*. Rather than a simple linear dependence on the circulation speed v_0, there is a turnover in cycle amplitude, at a speed which changes depending on the diffusivity in the convection zone. In the next section we investigate the cause of this behaviour in the model.

4. Advection versus Diffusion Dominated Solar Convection Zones

The turnover of cycle amplitude as depicted in Figure 5 occurs at a higher circulation speed v_0 as the diffusivity η_2 is increased. The asterisks (joined by a thin line) in Figure 7(a) show the location of this turnover as a function of η_2. We may think of this line in

the (η_2, v_0) plane as the dividing line between two distinct regimes of the dynamo, which we call *advection-dominated* and *diffusion-dominated*. The advection-dominated regime corresponds to high circulation speed and low diffusivity, while the diffusion-dominated regime corresponds to low circulation speed and high diffusivity. A shift from one of these regimes to another affects flux-transport dynamics in a way that results in contrasting dependence of cycle amplitude on the governing parameters. Consider how the cycle amplitude varies with v_0 for a fixed value of η_2, corresponding to a curve on Figure 5. In the diffusion-dominated regime, a higher circulation speed means less time for diffusive decay of the poloidal field during its transport through the convection zone, leading to more generation of toroidal field and hence a higher cycle amplitude. In the advection-dominated regime, a higher circulation speed leads to a lower cycle amplitude because there is less time to amplify toroidal field in the tachocline (through which magnetic fields are swept through at a faster speed). It is the balance between these conflicting influences that leads to a turnover in cycle amplitude at some intermediate circulation speed.

The bold line in Figure 7(a) shows the transition point between the two regimes that may be inferred from a simple balance between circulation and diffusion timescales $\tau_{\rm C}$ and $\tau_{\rm D}$. For a given circulation speed v_0, we define the circulation timescale $\tau_{\rm C}$ as the time taken for meridional circulation to advect poloidal fields from $r = 0.95R_\odot, \theta = 45^\circ$ to the location where the strongest toroidal field is formed at the tachocline ($\theta = 60^\circ$). The diffusion timescale is defined as $\tau_{\rm D} = L^2/\eta_2$, where $L = 0.285R_\odot$ is the radial distance across the convection zone from the same starting point. The two timescales are compared in Figure 7(b), where each horizontal line gives the circulation time $\tau_{\rm C}$ for a different speed v_0, and the bold curve gives $\tau_{\rm D}$ as a function of η_2. The crossing points of horizontal lines with this curve give the transition points between the advection dominated ($\tau_{\rm C} < \tau_{\rm D}$) and diffusion dominated ($\tau_{\rm C} > \tau_{\rm D}$) regimes from these simple theoretical considerations – which are in good agreement with the simulated transition points.

4.1. Magnetic Field Evolution in Advection versus Diffusion Dominated Regimes

We now compare the poloidal and toroidal field evolution in the two regimes. Figure 8 shows the poloidal field lines for two runs, at different times through the cycle, starting from one cycle minimum and finishing at the next cycle minimum, so that the fields reverse in sign. The left-hand column is taken from a run with $v_0 = 20\,{\rm m\,s^{-1}}$ and $\eta_2 = 0.5 \times 10^{12}\,{\rm cm^2\,s^{-1}}$, which is in the advection-dominated regime. The right-hand column is from a diffusion-dominated run with the same v_0 but with $\eta_2 = 2.0 \times 10^{12}\,{\rm cm^2\,s^{-1}}$. Figure 9 shows the

evolution of the toroidal field for the same two runs.

The key difference between the two regimes is the rate at which the poloidal field is able to diffuse through the convection zone, after it is generated at the surface by the Babcock-Leighton α-effect. This is seen clearly by comparing the poloidal field evolution between 8 and 12 years in the two runs (Figures 8c/h and d/i). In the diffusion-dominated run the new clockwise poloidal field diffuses directly down to the tachocline at all latitudes between these two times. However, in the advection-dominated run the new poloidal field does not reach the tachocline until the end of the cycle (16 years), and reaches the high latitudes before it reaches the tachocline; i.e., in this case, the field evolution follows the meridional circulation conveyor belt. There is still significant anticlockwise poloidal field remaining below the tachocline from the previous cycle, and even a lower band of clockwise field from the cycle before that. In the diffusion-dominated case there is only a weak band of anticlockwise field remaining from the previous cycle at solar minimum.

This suggests that in the advection-dominated regime, poloidal fields from cycles n, $n-1$, and $n-2$ combine to produce the toroidal field for cycle $n+1$, while in the diffusion-dominated regime it is produced primarily from cycle n poloidal field, with a small contribution from cycle $n-1$.

The main difference in toroidal field evolution seen in Figure 9 is during the rising phase of the cycle, seen at 4 and 8 years (panels b/g and c/h). In the advection-dominated regime there are two separate regions of toroidal field generation, one region at high latitudes from poloidal field which has been advected poleward by the meridional circulation, and a second region at lower latitudes arising from direct diffusion of poloidal field across the convection zone. In the diffusion-dominated case there is no strong generation of toroidal field at high latitudes. In this case the strongest field generation occurs at mid to low latitudes, with direct diffusion presumably being the primary means of transporting poloidal field to the base of the convection zone (i.e., the meridional circulation conveyor belt is "short-circuited"). We point our however that, contrary to usual expectations, diffusive flux transport still plays a role in the advection-dominated case, and it is responsible for the complex dependence of cycle amplitude on diffusivity in the advection-dominated regime; we explore this issue below.

4.2. The Role of Diffusive Flux Transport

We have thus far identified the turnover in cycle amplitude to lie at the transition point between advection-dominated and diffusion-dominated regimes of the dynamo. Within the

umbrella of this model, this maximum in the amplitude is understood to be a balance between the time available for toroidal field amplification and the time available for poloidal field decay. Figure 6 shows how the cycle amplitude varies with the diffusivity η_2 for a fixed circulation speed v_0. We see that there is a turnover in cycle amplitude for some value of η_2, with lower diffusivities corresponding to the advection-dominated regime, and higher diffusivities to the diffusion-dominated regime. In the diffusion-dominated regime, which is only reached for lower speeds v_0 in Figure 6, the cycle amplitude decreases with increasing diffusivity. This is expected due to increased cancellation and decay of the poloidal field. However, in the advection-dominated regime, the cycle amplitude *increases* as the diffusivity η_2 is increased. This initially seems counter-intuitive, but we show here that it is caused by the influence of direct diffusive flux transport of poloidal field across the convection zone.

This direct diffusion (from the solar surface to the base of the SCZ) was visible in the poloidal field evolution plots shown in the previous section; we now demonstrate its quantitative effect as η_2 is varied, by comparing the poloidal field strength $|\mathbf{B}_\mathrm{p}|$ at the base of the convection zone ($r = 0.715 R_\odot$) with that at the solar surface ($r = R_\odot$). We take the ratio $|\mathbf{B}_\mathrm{p}(\mathrm{base})| \,/\, |\mathbf{B}_\mathrm{p}(\mathrm{top})|$, using the peak value of $|\mathbf{B}_\mathrm{p}|$ at each location during the solar cycle. This ratio is plotted in Figure 10, measured at latitudes 30° and 60°, and for two different circulation speeds. Thin lines correspond to $v_0 = 30\,\mathrm{m\,s^{-1}}$, where the dynamo is in the advection-dominated regime for the whole range of η_2 shown. Thick lines correspond to $v_0 = 20\,\mathrm{m\,s^{-1}}$, for which the dynamo changes between the two regimes at about $\eta_2 = 1.1 \times 10^{12}\,\mathrm{cm^2\,s^{-1}}$.

Consider first the behaviour at 30° latitude (solid lines in Figure 10). Here the curves for both v_0 have positive slope, which implies that a greater proportion of poloidal field from the surface reaches the bottom of the convection zone as η_2 is increased. Thus direct diffusive flux transport at lower latitudes always acts to increase the amount of poloidal field reaching the base of the convection zone. Nearer to the pole, at 60° latitude (dashed lines in Figure 10), the behaviour is different. Here the ratio decreases as η_2 is increased, both for the curve with $v_0 = 30\,\mathrm{m\,s^{-1}}$ and in the diffusion-dominated regime for $v_0 = 20\,\mathrm{m\,s^{-1}}$. In the advection-dominated regime for $v_0 = 20\,\mathrm{m\,s^{-1}}$ however, the ratio first increases with η_2. This suggests a more complex relation between the surface and tachocline poloidal fields at high latitude, with competing influence from both diffusive and advective flux transport. This is expected because the downflow in the circulation is located at high latitudes.

The analysis presented in this section supports the idea that direct diffusive transport of poloidal field across the convection zone, especially around mid-latitudes, is responsible for the trend of increasing cycle amplitude with increasing diffusivity, found in the advection-dominated regime. Although such diffusive transport acts to increase cycle amplitude in

both regimes, diffusion also causes the poloidal field that is being transported by meridional circulation to decay, cancelling with field from the previous cycle that is stored below the tachocline. Thus diffusion also has a negative effect on cycle amplitude. It is this negative effect which dominates at higher diffusivities, forcing the dynamo into the diffusion-dominated regime where cycle amplitude decreases with increasing diffusivity.

5. Persistence of Memory: Cycle-to-Cycle Correlations in Advection versus Diffusion Dominated Regimes in a Stochastically Forced Dynamo

It is expected that the memory of a flux-transport dynamo is much longer in the advection-dominated regime than in the diffusion-dominated regime, and solar cycle predictions have been based on this expectation (Dikpati & Gilman 2006; Jiang et al. 2007). However, a detailed comparative analysis of persistence of memory in these different regimes under the umbrella of the same model had not been previously performed. Our analysis in the previous section has brought us closer to understanding the flux transport dynamics (in these two regimes) that is the physical basis for any memory mechanism. In this section, we consider how the persistence of this memory differs between the two regimes, by looking at the correlation between peak polar and toroidal fields of subsequent cycles. Since the simulations considered earlier relaxed to a regular periodic cycle, we cannot use these to study correlations between different cycles. Therefore, we now introduce self-consistent fluctuations in the cycle properties by means of a stochastically varying α-effect, and explore the resulting correlations between different cycles.

5.1. Stochastic Fluctuations

We introduce fluctuations in the model by varying the coefficient α_0 of the α-effect (see Chatterjee et al. 2004 for the full expression). We set

$$\alpha_0 = \alpha_{\rm base} + \alpha_{\rm fluc}\,\sigma(t;\tau_{\rm cor}), \tag{10}$$

where $\alpha_{\rm base} = 30\,{\rm m\,s^{-1}}$ is the mean value, $\alpha_{\rm fluc} = 30\,{\rm m\,s^{-1}}$ gives the maximum amplitude of the fluctuations (corresponding to the 200% level), and σ is a uniform random deviate selected from the interval $[-1, 1]$, with a new value after each coherence time $\tau_{\rm cor}$. Although for our purposes this is essentially a device for changing the cycle properties from one cycle to the next, there is a strong physical basis for stochastic variations in α which have been invoked in several previous studies (Choudhuri 1992; Hoyng 1993; Ossendrijver et al. 1996; Charbonneau & Dikpati 2000; Mininni & Gómez 2002). Our model uses a Babcock-Leighton

α-effect where poloidal field is generated at the surface from the decay of tilted active regions (Babcock 1961; Leighton 1969). Thus stochastic variations in the α coefficient are natural, because it arises from the cumulative effect of a finite number of discrete flux emergence events (active region eruptions with varying degrees of tilt).

To compare the two regimes we consider two runs, both with $\eta_2 = 1.0 \times 10^{12}\,\mathrm{cm^2\,s^{-1}}$. The circulation speed v_0 is kept constant throughout each run, and only the α effect is varied. Run 1 has $v_0 = 15\,\mathrm{m\,s^{-1}}$, so is diffusion-dominated, while run 2 has $v_0 = 26\,\mathrm{m\,s^{-1}}$ and is advection-dominated. The coherence time τ_{cor} is set to 2.3 years in run 1 and 1.5 years in run 2, so as to keep the ratio of the former to the cycle duration roughly the same in each case. We note that although the exact value of the coherence time is not important for our study (and is introduced just as a means to enable sufficient fluctuations), the timescale – on the order of a year – is chosen to reflect that the BL α-effect is a result of surface flux transport processes (diffusion, meridional circulation and differential rotation) which can take up to a year to generate a net radial (component of the poloidal) field from multiple flux emergence events (Mackay et al. 2004).

5.2. Correlation Analysis

In this section we compare the peak surface radial flux Φ_r for cycle n with the peak toroidal flux Φ_{tor} for cycles n, $n+1$, $n+2$, and $n+3$. The toroidal flux is defined as before by integrating $B(r,\theta)$ over the region $r = 0.677R_\odot$ to $0.726R_\odot$, $\theta = 45^\circ$ to 80°. The radial flux Φ_r is found by integrating $B_r(R_\odot,\theta)$ over the solar surface between $\theta = 1^\circ$ to 20°, (i.e., latitudes 70° to 89°). Note that the peak toroidal flux precedes the peak surface radial flux for the same cycle, which has the same sign. The poloidal field then produces the toroidal field for cycle $n+1$ with the opposite sign. We measure the correlation of the surface radial flux for cycle n with the toroidal flux of different cycles, comparing the absolute value of each total signed flux.

Both runs were computed for a total of 275 cycles with fluctuating α_0, so as to produce meaningful statistics for each of the dynamo regimes. The results are illustrated in Figures 11 and 12 as scatter-plots of Φ_{tor} for different cycles against $\Phi_r(n)$. The (non-parametric) Spearman's rank correlation coefficient r_{s} is given above each plot, along with its significance level. The correlation coefficients are summarised in Table 1, where the Pearson's linear correlation coefficient r_{p} is also given for comparison. Although the latter is less reliable, as it assumes a linear relation, it agrees well with r_{s} in each case.

The results show a clear difference between the two regimes. The advection-dominated

regime shows significant correlations at all 4 time delays, apparently suggesting that the memory of past poloidal field survives for at least 3 cycles; however, more on this later. The diffusion-dominated regime has a strong correlation only between $\Phi_r(n)$ and $\Phi_{\rm tor}(n+1)$, suggesting that the dominant memory relates to just a one cycle time-lag, although very weak correlations are also found with $\Phi_{\rm tor}(n)$ and $\Phi_{\rm tor}(n+3)$.

In both regimes the strongest relation is the positive correlation between $\Phi_r(n)$ and $\Phi_{\rm tor}(n+1)$. This is to be expected as this is the more deterministic phase of the cycle – where toroidal fields (of cycle $n+1$, say) are inducted from the older cycle n poloidal field via the relatively steady differential rotation. Note however that the two fluxes do not have to be directly coupled, in that the two fluxes may be positively correlated because they are both created from the mid-latitude poloidal field of cycle n (generated by the α-effect). The polar flux $\Phi_r(n)$ arises through poleward meridional transport of the cycle n poloidal field, while the toroidal flux $\Phi_{\rm tor}(n+1)$ is generated from cycle n poloidal field that is diffusively transported across the convection zone. This is particularly the case in the diffusion-dominated regime. Nonetheless, even this indirect scenario suggests that the strongest correlation should in fact be between the cycle n poloidal field and cycle $n+1$ toroidal field in this class of α-Ω dynamo models.

The other phase of the cycle, in which the poloidal field is generated by the α-effect, is inherently more random due to the fluctuating α-effect in these runs. Nevertheless, there is a strong positive correlation between $\Phi_{\rm tor}(n)$ and $\Phi_r(n)$ in the advection-dominated regime, while this correlation is largely absent in the diffusion-dominated regime. This we attribute to the relatively stronger role of advective flux transport in the advection-dominated regime – which implies that a larger fraction of the original toroidal flux that has buoyantly erupted is transported to the polar regions by the circulation. In effect therefore, the advection-dominated regime allows correlations to propagate *in both phases of the cycle*, whereas the diffusion-dominated case allows correlations to propagate only in the poloidal-to-toroidal phase. The other correlation is broken in the diffusion-dominated regime because the advection is short-circuited by direct diffusion, which transports flux downwards and equatorward – where it is cancelled by oppositely signed flux from the other hemisphere. This explains how the correlations can survive for multiple cycles in the advection-dominated regime, but not in the diffusion-dominated regime.

6. Conclusion

Significant uncertainties remain in our understanding of the physics of the solar dynamo mechanism, implying that prediction of future solar activity based on physical models is a

challenging task. Here we have demonstrated how a flux-transport dynamo model behaves differently in advection and diffusion dominated regimes. Such differences, amongst others, have previously led to conflicting predictions of the amplitude of Cycle 24. Dikpati et al. (2006) use an advection-dominated model to predict a much stronger cycle than Cycle 23, whereas Choudhuri et al. (2007) use a diffusion-dominated model to predict a much weaker cycle. The latter prediction is somewhat similar in spirit to the precursor methods (Schatten 2005; Svalgaard et al. 2005), which use the polar field at cycle minimum to predict the amplitude of the following cycle. Owing to the lack of observations of conditions inside the convection zone, opinions differ as to whether the real solar dynamo is weakly or strongly diffusive (e.g. Dikpati & Gilman 2006; Jiang et al. 2007).

We find that for low circulation speeds v_0 (in the diffusion-dominated regime), the cycle amplitude is an increasing function of v_0, as in the observations of Hathaway et al. (2003). However, the amplitude curve has a turnover point and is a decreasing function of v_0 at higher v_0 (in the advection-dominated regime), opposite to the observed correlation. When the diffusivity in the convection zone is increased, the location of this turnover moves to a higher v_0. Our extensive analysis shows that this turnover corresponds to the transition between the diffusion and advection dominated regimes. In the diffusion-dominated regime, faster circulation means less time for decay of the poloidal field, leading to a higher cycle amplitude, whereas in the advection-dominated regime diffusive decay is less important and a faster circulation means less time to induct toroidal field, thus generating a lower cycle amplitude. If the observed statistics of the past 12 cycles as reported by Hathaway et al. (2003) reflect a true underlying trend, then our results imply that the solar dynamo is in fact working in a regime which is dominated by diffusive flux transport in the main body of the SCZ (although the cycle period is still governed by the slow meridional circulation counterflow at the base of the SCZ). This conclusion supports the analysis of Jiang et al. (2007).

Through a correlation analysis in a stochastically forced version of our model, we have also explored the persistence of memory in the solar cycle for both the diffusion-dominated and advection-dominated regimes. It is this memory mechanism which is understood to lead to predictive capabilities in α-Ω dynamo models with spatially segregated source regions for the α and Ω effects. This understanding is based on the finite time delay required for flux transport to communicate between these different source regions. We find that the polar field of cycle n correlates strongest with the amplitude (toroidal flux) of cycle $n+1$ in both the regimes. In the diffusion-dominated regime this is the only significant correlation, indicative of a one-cycle memory only. However, in the advection-dominated case, there are also significant correlations with the amplitude of cycles n, $n+2$, and $n+3$. In contrast to the correlations that we infer, Charbonneau & Dikpati (2000) found that the strongest

correlation in their advection dominated model was with a two-cycle time lag. Since such correlations lead to predictive capabilities, and obviously seem to be model and parameter-dependent as suggested by our results, such a correlation analysis should be the first step towards any prediction, the latter being based on the former. In hindsight, however, both Dikpati et al. (2006) – who use an advection-dominated model and inputs from multiple previous cycles, and Choudhuri et al. (2007) – who use a diffusion-dominated model and input from only the past cycle to predict the next cycle, appear to be have made the correct choices within their modelling assumptions.

Note that the memory mechanism in our advection-dominated case appears to have a different cause than that implied by Dikpati & Gilman (2006), who invoke the survival of multiple old-cycle polar fields feeding into a new cycle toroidal field. All of the surviving correlations in our advection-dominated regime (Figure 12) are positive; they do not alternate in sign. This alternation in sign would be expected if bands of multiple older cycle poloidal field survive in the tachocline – odd and even cycle poloidal fields would obviously contribute oppositely because of their alternating signs. In that case we would expect the absolute value of $\Phi_r(n)$ to correlate positively with $\Phi_{\rm tor}(n+1)$ and $\Phi_{\rm tor}(n+3)$ and so on, but negatively with $\Phi_{\rm tor}(n+2)$ and $\Phi_{\rm tor}(n+4)$ and so on, as evident in the results of Charbonneau & Dikpati (2000, Figure 9; after accounting for the fact that they use signed magnetic fields). Rather, in the advection-dominated regime of our model, the correlations appear to persist simply because fluctuations in field strength are passed on in both the poloidal-to-toroidal and toroidal-to-poloidal phases of the cycle, as evidenced by the correlation between amplitude and polar flux of cycle n. In a recent analysis, Cameron & Schüssler (2007) find that the predictive skill of a surface flux transport model – similar in spirit to the advection-dominated dynamo model of Dikpati et al. (2006) – is contained in the input information of sunspot areas in the declining phase of the cycle. They argue that memory of multiple past cycles, in the form of surviving bands of poloidal field (its surface manifestations in their case), need not be the only reason behind the predictive capability of the advection-dominated dynamo model of Dikpati et al. (2006). Our analysis of the advection-dominated regime supports this suggestion of Cameron & Schüssler (2007).

Coming back to the diffusion-dominated regime, our comparative analysis indicates that in this case, the memory of past cycles is governed by downward diffusion of poloidal field into the tachocline – which primarily results in a one-cycle memory. The fact that diffusion is an efficient means for transporting flux is often ignored, especially in this era of advection-dominated models; however, we find that diffusive flux transport is quite efficient. The identification of this one cycle memory in our stochastically forced model contradicts Dikpati & Gilman (2006) – who claim that prediction is not possible in this regime. As long as the source regions are spatially segregated, and one of the source effects is observable and

the other deterministic, flux transport α-Ω dynamos will inherently have predictive skills no matter what physical process (i.e., circulation, or diffusion, or downward flux-pumping) is invoked to couple the two regions. We may also point out that in the context of cycle-to-cycle correlations, downward flux pumping (Tobias et al. 2001) would have the same effect as diffusion in that it also acts to short-circuit the meridional circulation conveyor belt. So although downward flux pumping differs from diffusive transport because in the latter case the fields may reduce in strength due to decay, the overall persistence of memory is expected to be similar if diffusive flux transport was replaced or complemented by downward flux pumping.

In summary, our analysis has served both to explore the diffusion dominated and advection dominated regimes within the framework of a BL type dynamo, and to demonstrate how the memory of the dynamo may be different in these two regimes. Based on our analysis we assert that diffusive flux transport in the SCZ plays an important role in flux transport dynamics, even if the dynamo cycle period is governed by the meridional flow speed. In fact, the observed solar cycle amplitude-period dependence may arise more naturally in the diffusion-dominated regime, as discussed earlier. Taken together therefore, we may conclude that diffusive flux transport is a significant physical process in the dynamo mechanism and this process leads primarily to a one-cycle memory which may form the physical basis for solar cycle predictions, if other physical mechanisms involved in the complete dynamo chain of events are well understood. Separate, detailed examinations of these other related physical mechanisms will be performed in the future.

This research was funded by NASA Living With a Star grant NNG05GE47G. We also acknowledge support from the UK STFC and the Solar Physics NSF-REU program at Montana State University.

REFERENCES

Babcock, H. W. 1961, ApJ, 133, 572

Beer, J. 2000, Space Sci. Rev., 94, 53

Beer, J., Tobias, S., & Weiss, N. 1998, Sol. Phys., 181, 237

Bonanno, A., Elstner, D., Rüdiger, G., & Belvedere, G. 2002, A&A, 390, 673

Cameron, R., & Schüssler, M. 2007, ApJ, 659, 801

Charbonneau, P. 2005, Living Rev. Sol. Phys., 2, 2, http://solarphysics.livingreviews.org/Articles/lrsp-2005-2/

Charbonneau, P., & Dikpati, M. 2000, ApJ, 543, 1027

Charbonneau, P., St-Jean, C., & Zacharias, P. 2005, ApJ, 619, 613

Chatterjee, P., & Choudhuri, A. R. 2006, Sol. Phys., 239, 29

Chatterjee, P., Nandy, D., & Choudhuri, A. R. 2004, A&A, 427, 1019

Choudhuri, A. R. 1992, A&A, 253, 277

Choudhuri, A. R. 2003, Sol. Phys., 215, 31

Choudhuri, A. R., Chatterjee, P., & Jiang, J. 2007, Phys. Rev. Lett., 98, 131103

Choudhuri, A. R., Schüssler, M., & Dikpati, M. 1995, A&A, 303, L29

Dikpati, M., & Charbonneau, P. 1999, ApJ, 518, 508

Dikpati, M., de Toma, G., & Gilman, P. A. 2006, Geophys. Res. Lett., 33, 5102

Dikpati, M., & Gilman, P. A. 2006, ApJ, 649, 498

Durney, B. R. 1995, Sol. Phys., 160, 213

Durney, B. R. 2000, Sol. Phys., 196, 421

Hathaway, D. H. 1996, ApJ, 460, 1027

Hathaway, D. H. 2005, in ASP Conf. Ser. 346, Large-scale Structures and their Role in Solar Activity, ed. K. Sankarasubramanian, M. Penn, & A. Pevtsov (San Francisco, ASP), 19

Hathaway, D. H., Nandy, D., Wilson, R. M., & Reichmann, E. J. 2003, ApJ, 589, 665

Hoyng, P. 1993, A&A, 272, 321

Jiang, J., Chatterjee, P., & Choudhuri, A.R. 2007, MNRAS, submitted

Knobloch, E., Tobias, S. M., & Weiss, N. O. 1998, MNRAS, 297, 1123

Küker, M., Arlt, R., & Rüdiger, G. 1999, A&A, 343, 977

Küker, M., Rüdiger, G., & Schultz, M. 2001, A&A, 374, 301

Leighton, R. B. 1969, ApJ, 156, 1

Mackay, D. H., Jardine, M., Collier Cameron, A., Donati, J.-F, & Hussain, G. A. J. 2004, MNRAS, 354, 737

Miesch, M. S. 2005, Living Rev. Sol. Phys., 2, 1, http://solarphysics.livingreviews.org/Articles/lrsp-2005-1/

Mininni, P. D., & Gómez, D. O. 2002, ApJ, 573, 454

Moffatt, H. K. 1978, Magnetic Field Generation in Electrically Conducting Fluids (Cambridge: Cambridge Univ. Press)

Nandy, D. 2004, in Proceedings of SOHO 14/GONG 2004, Helio- and Asteroseismology: Towards a Golden Future, ed. D. Danesy (ESA SP-599), 241

Nandy, D., & Choudhuri, A. R. 2001, ApJ, 551, 576

Nandy, D., & Choudhuri, A. R. 2002, Science, 296, 1671

Nandy, D., &, Martens, P.C.H. 2007, Adv. Space Res., in press

Ossendrijver, A. J. H., Hoyng, P., & Schmitt, D. 1996, A&A, 313, 938

Ossendrijver, M. 2003, A&A Rev., 11, 287

Parker, E. N. 1955, ApJ, 121, 491

Schatten, K. 2005, Geophys. Res. Lett., 32, 21106

Schüssler, M., & Schmitt, D. 2004, A&A, 421, 349

Sheeley, N. R. 1991, ApJ, 374, 386

Solanki, S. K., Krivova, N. A., Schüssler, M., & Fligge, M. 2002, A&A 396, 1029

Svalgaard, L., Cliver, E. W., & Kamide, Y. 2005, Geophys. Res. Lett., 32, 1104

Tobias, S. M. 1997, A&A, 322, 1007

Tobias, S. M., Brummell, N. H., Clune, T. L., Toomre, J. 2001, ApJ, 549, 1183

Wang, Y.-M., Lean, J., & Sheeley, N. R. 2002, ApJ, 577, L53

Wilmot-Smith, A. L., Martens, P. C. H., Nandy, D., Priest, E. R., & Tobias, S. M. 2005, MNRAS, 363, 1167

Wilmot-Smith, A. L., Nandy, D., Hornig, G., & Martens, P. C. H. 2006, ApJ, 652, 696

Yoshimura, H. 1978, ApJ, 226, 706

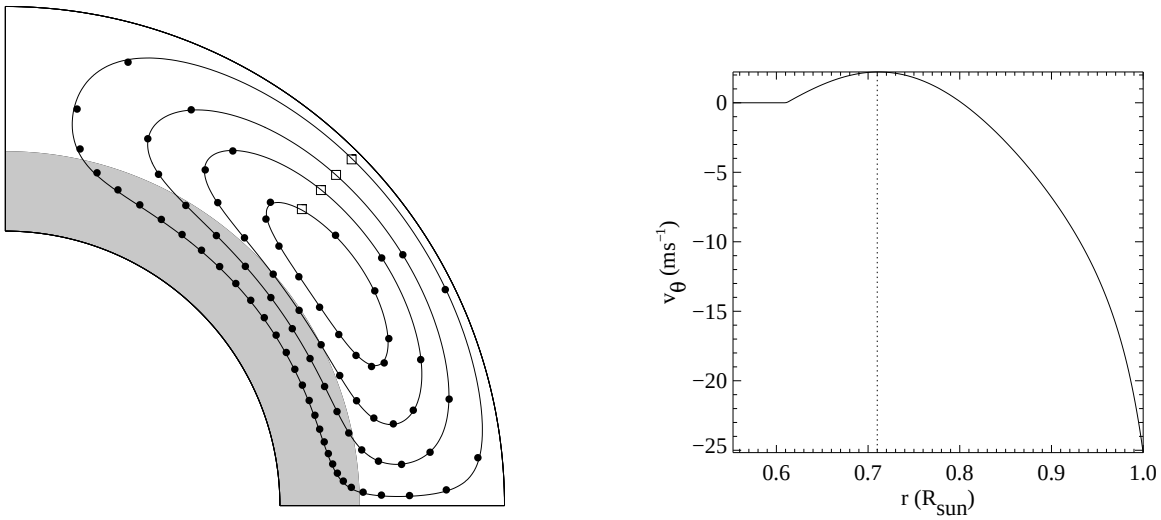

Fig. 1.— Streamlines of the meridional circulation profile in our model (*left*), and latitudinal velocity profile across a radial cut at $\theta = 45°$ (*right*). Dots on the streamlines show yearly positions for particles with $v_0 = 25\,\mathrm{m\,s^{-1}}$, starting from the squares at $\theta = 45°$ and moving anti-clockwise.

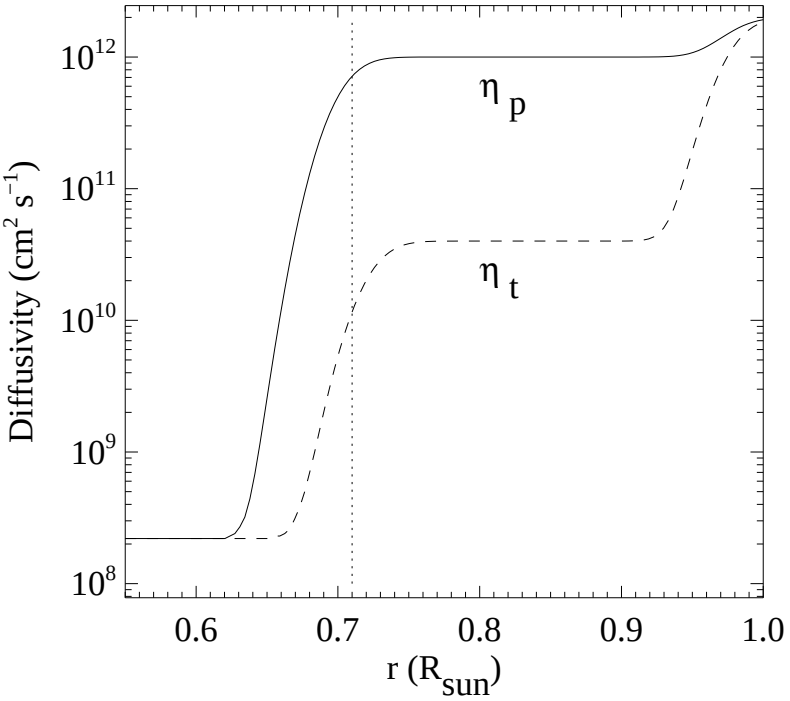

Fig. 2.— Example diffusion profiles as a function of r for the toroidal (η_t) and poloidal (η_p) fields. The dotted line shows the location of the tachocline. Here $\eta_0 = 2.0 \times 10^{12}\,\mathrm{cm^2\,s^{-1}}$, $\eta_1 = 0.04 \times 10^{12}\,\mathrm{cm^2\,s^{-1}}$, and $\eta_2 = 1.0 \times 10^{12}\,\mathrm{cm^2\,s^{-1}}$.

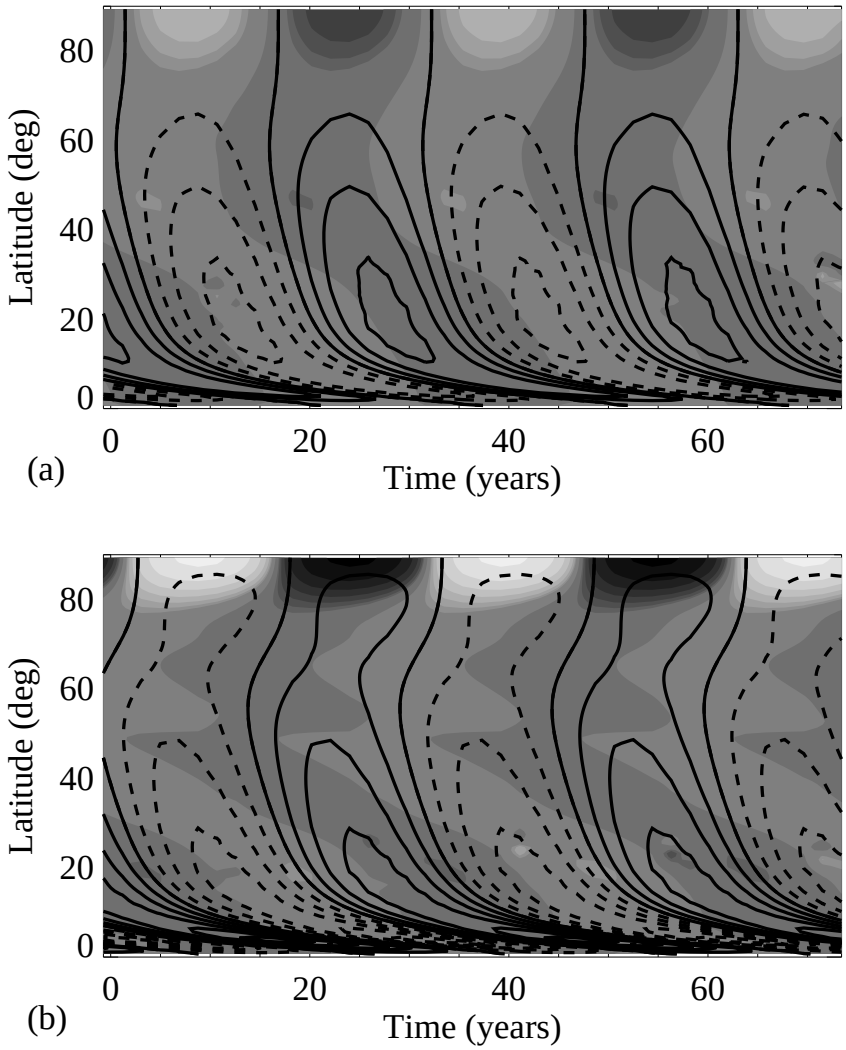

Fig. 3.— Two example solutions: (a) with $v_0 = 20\,\mathrm{m\,s^{-1}}$ and $\eta_2 = 2.0 \times 10^{12}\,\mathrm{cm^2\,s^{-1}}$ (characterizing a diffusive flux-transport dominated SCZ); and (b) with the same v_0 but $\eta_2 = 0.5 \times 10^{12}\,\mathrm{cm^2\,s^{-1}}$ (characterizing an advective flux-transport dominated SCZ). In each case black lines are contours of toroidal field B at the base of the convection zone (solid lines for positive values, dashed for negative). The grayscale in the background shows surface radial field strength $B_r(r = R_\odot)$, with white for positive and black for negative. The same contour levels are used in both plots.

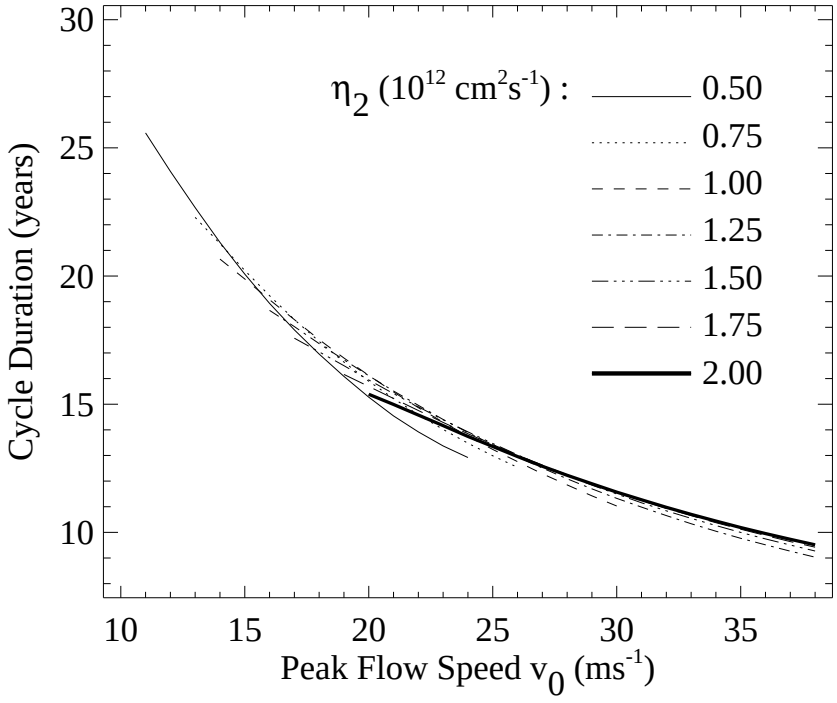

Fig. 4.— Dependence of cycle duration on the meridional circulation speed v_0. Each line style corresponds to a different value of η_2 (the poloidal diffusivity in the convection zone) as given in the legend.

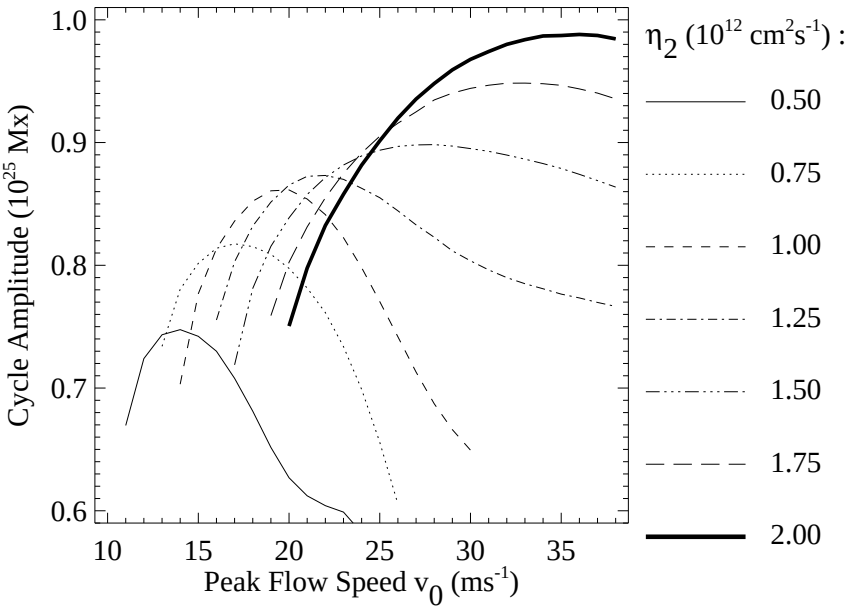

Fig. 5.— Dependence of cycle amplitude on the meridional circulation speed v_0. Each line style corresponds to a different value of η_2 (the poloidal diffusivity in the convection zone) as given in the legend.

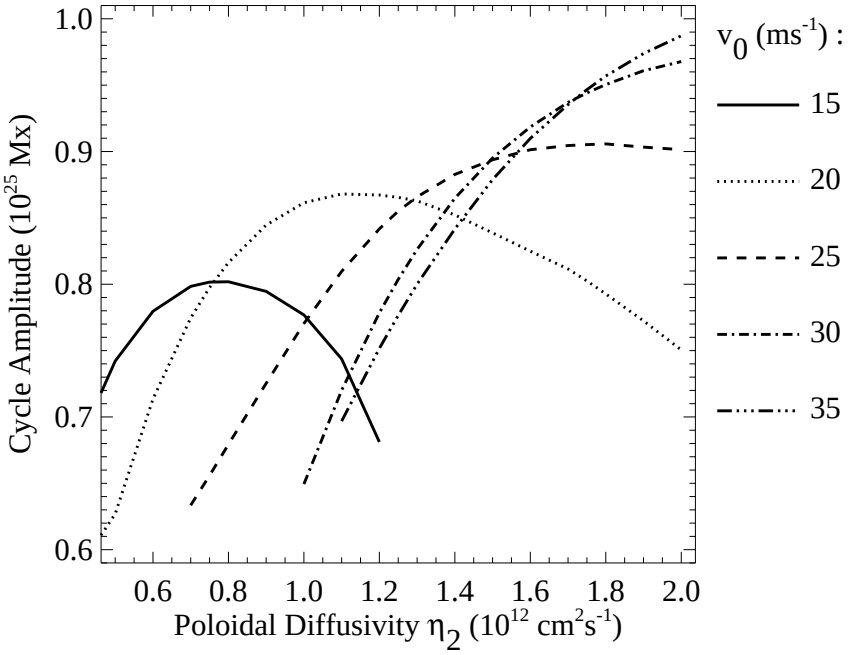

Fig. 6.— Dependence of cycle amplitude on the poloidal diffusivity η_2 in the convection zone. Each line style corresponds to a different value of the meridional circulation speed v_0, as given in the legend.

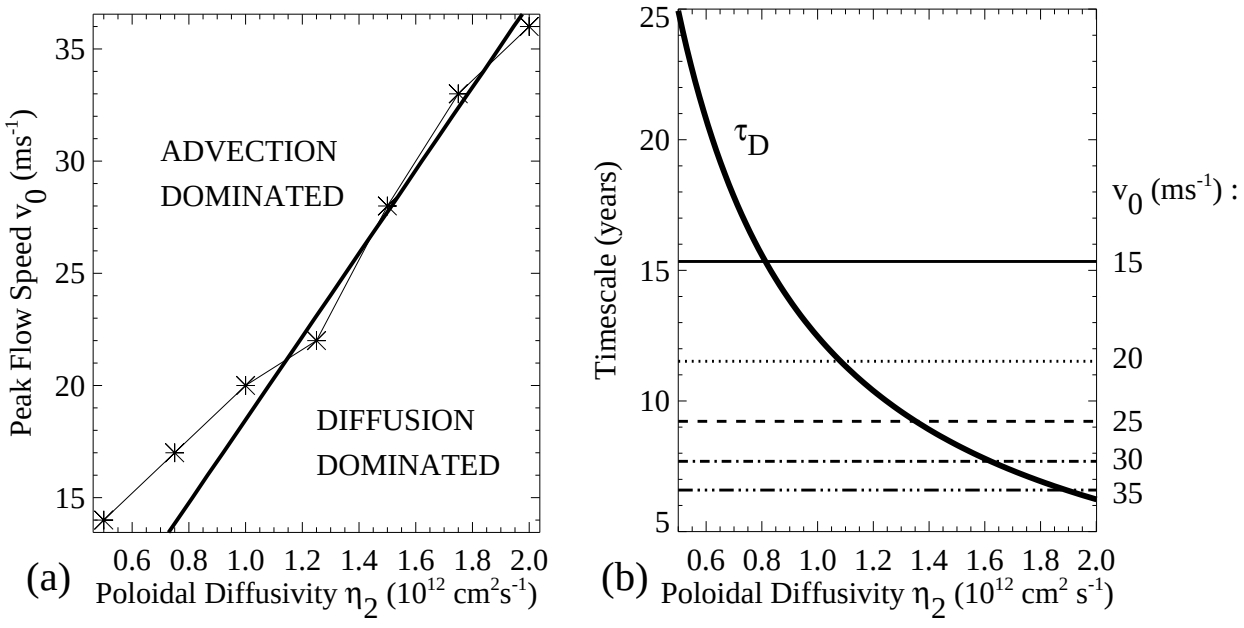

Fig. 7.— Transition between the advection-dominated and diffusion-dominated regimes. In (a) asterisks indicate the flow speeds v_0 corresponding to turnover of cycle amplitude for fixed values of η_2 (inferred from the simulations shown in Figures 5 and 6). The bold line shows the transition point that may be inferred from simple theoretical comparison of circulation and diffusion timescales. Panel (b) shows the diffusion timescale $\tau_{\rm D}$ as a function of η_2 (bold line), and circulation timescales $\tau_{\rm C}$ for selected speeds v_0 (horizontal lines), as defined in the text.

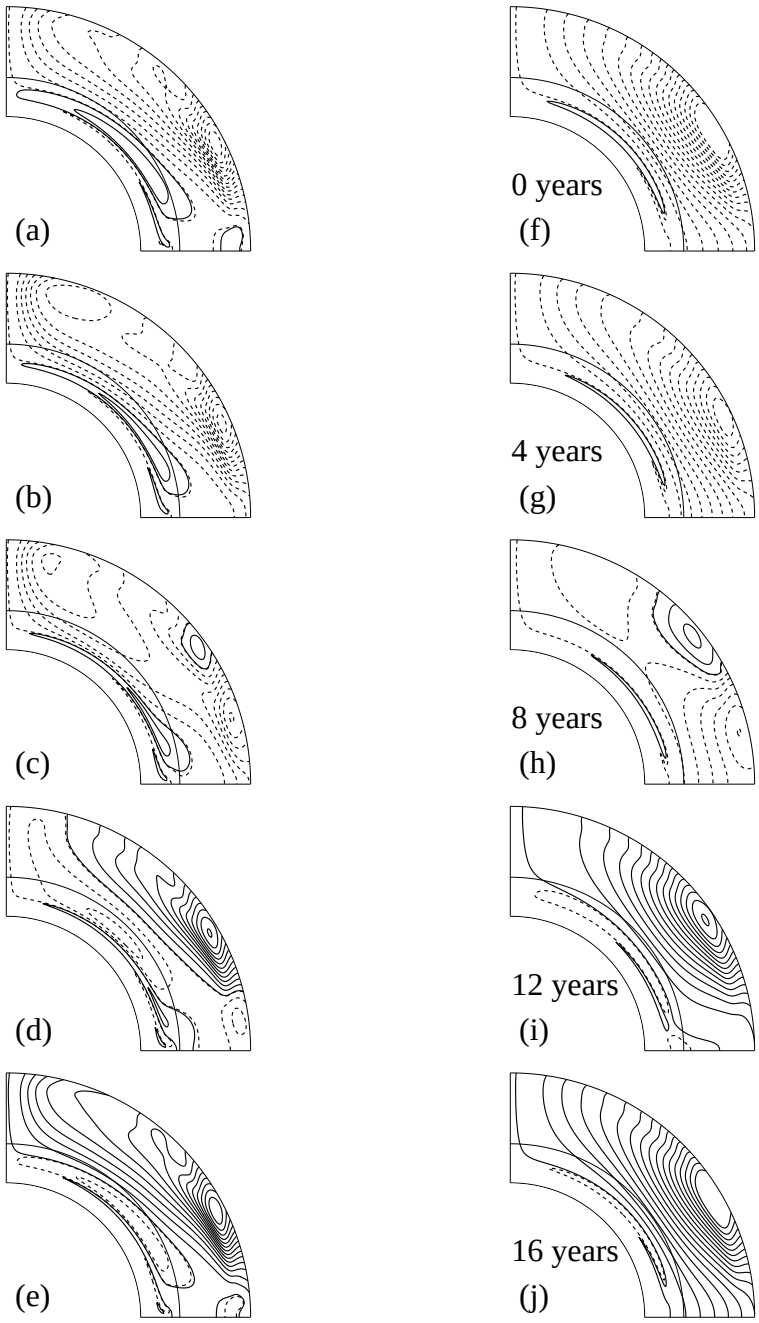

Fig. 8.— Comparison of poloidal fields in advection-dominated (left column/panels a to e) and diffusion-dominated (right column/panels f to j) regimes. Each row corresponds to a time through the solar cycle, running from one cycle minimum to the next. Solid lines show clockwise field lines and dashed lines show anti-clockwise field lines. Also indicated is the base of the SCZ at $0.71R_{\odot}$.

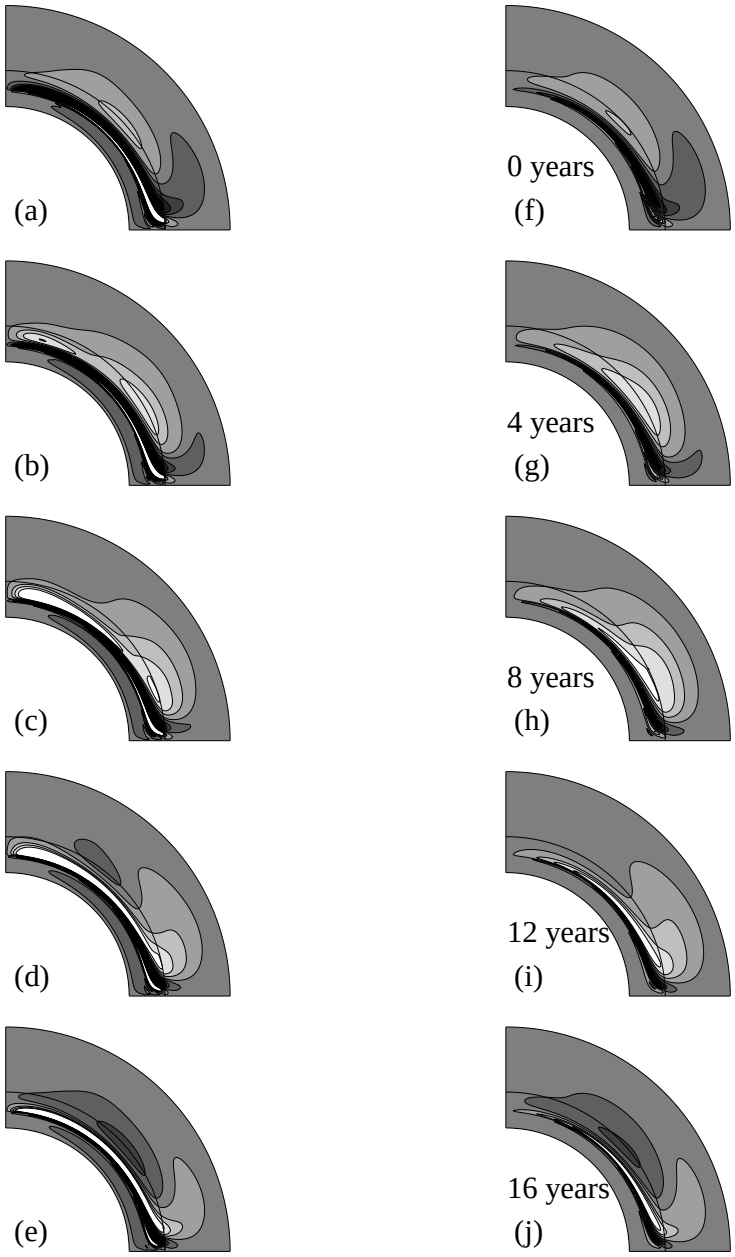

Fig. 9.— Comparison of toroidal field in advection-dominated (left column/panels a to e) and diffusion-dominated (right column/panels f to j) regimes. Each row corresponds to a different time through the solar cycle, running from one cycle minimum to the next. Grayscale contours show toroidal field strength, with black corresponding to the strongest negative field and white to the strongest positive toroidal field. Also indicated is the base of the SCZ at $0.71R_{\odot}$.

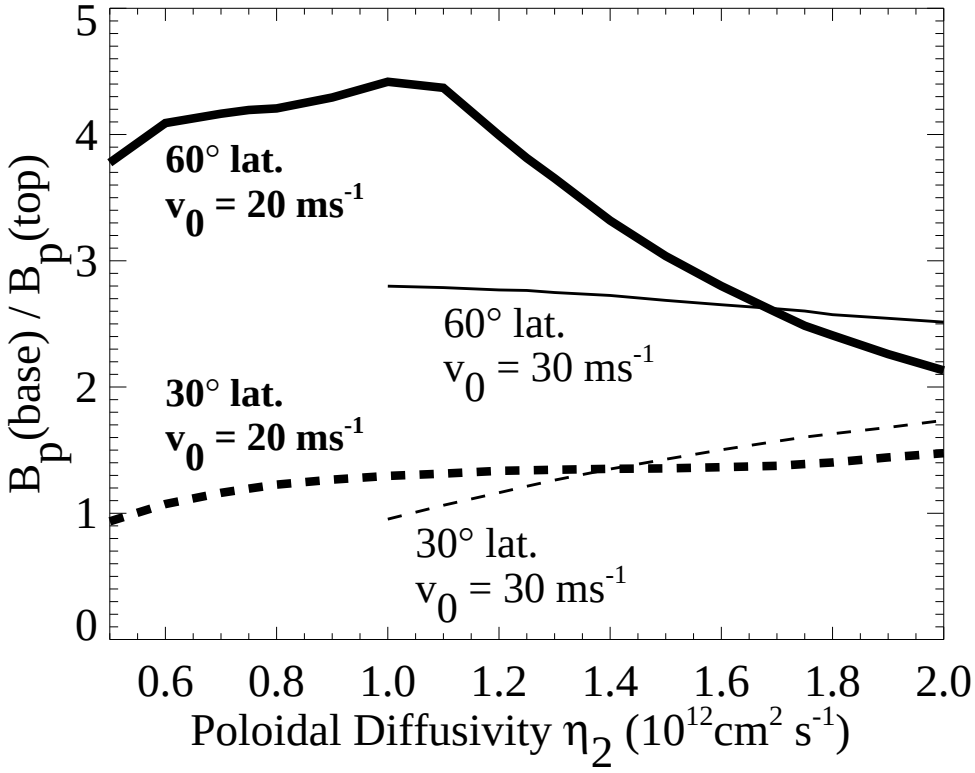

Fig. 10.— Ratio of poloidal field $|\mathbf{B}_\mathrm{p}|$ at base of convection zone ($r = 0.715 R_\odot$) to that at the surface ($r = R_\odot$), measured as a function of diffusivity at latitudes 30° (solid lines) and 60° (dashed lines). Thick lines correspond to runs with $v_0 = 20\,\mathrm{m\,s^{-1}}$ and thin lines to runs with $v_0 = 30\,\mathrm{m\,s^{-1}}$.

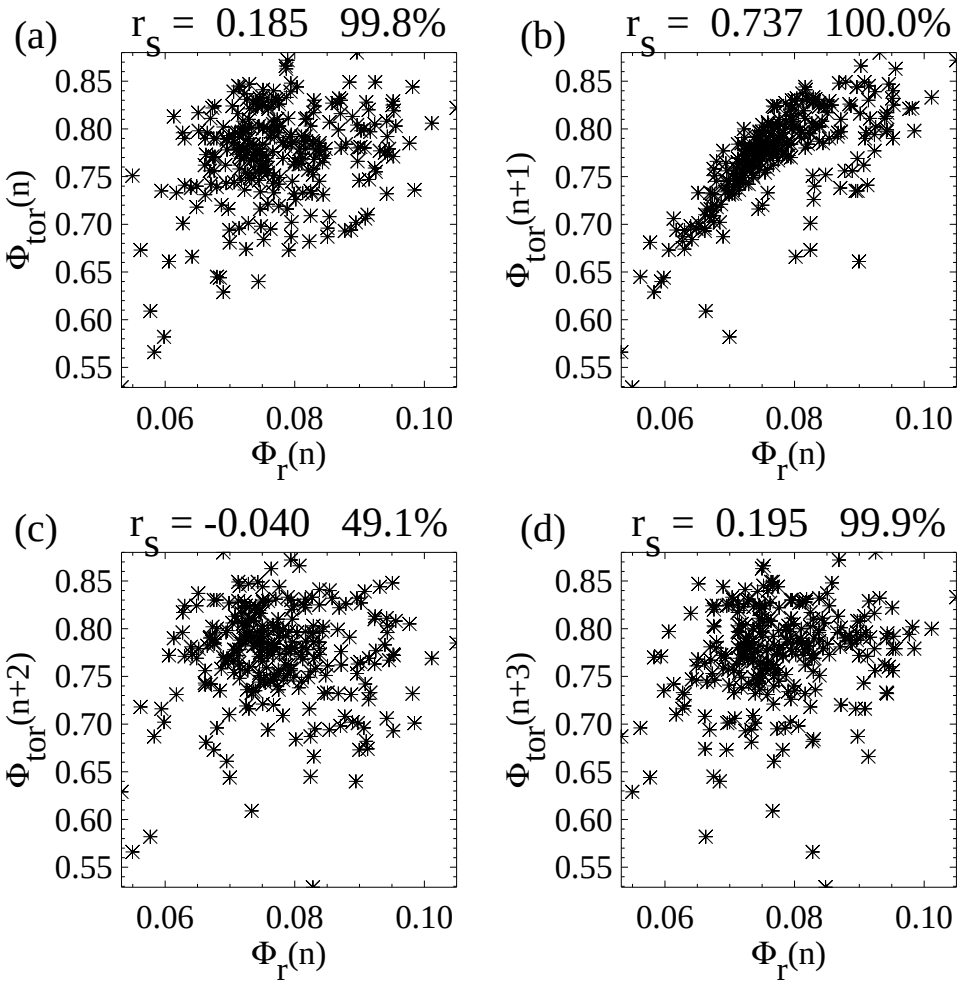

Fig. 11.— Cycle-to-cycle correlations in the diffusion-dominated regime (run 1), between radial flux $\Phi_r(n)$ and (a) toroidal flux $\Phi_{\rm tor}(n)$, (b) $\Phi_{\rm tor}(n+1)$, (c) $\Phi_{\rm tor}(n+2)$, and (d) $\Phi_{\rm tor}(n+3)$. The Spearman's rank correlation coefficient is given along with its significance level for 275 cycles. All magnetic fluxes are in units of 10^{25} Mx.

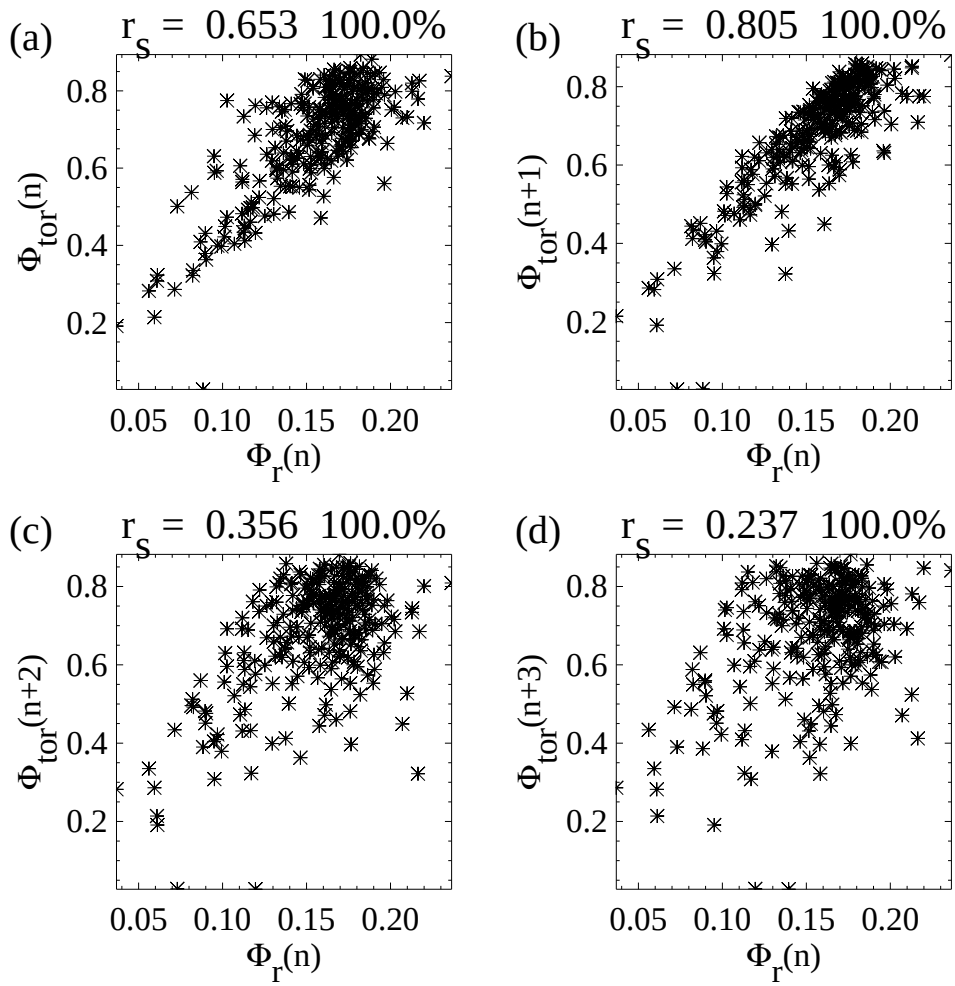

Fig. 12.— Cycle-to-cycle correlations in the advection-dominated regime (run 2), between radial flux $\Phi_r(n)$ and (a) toroidal flux $\Phi_{\rm tor}(n)$, (b) $\Phi_{\rm tor}(n+1)$, (c) $\Phi_{\rm tor}(n+2)$, and (d) $\Phi_{\rm tor}(n+3)$. The Spearman's rank correlation coefficient is given along with its significance level for 275 cycles. All magnetic fluxes are in units of 10^{25} Mx.

Table 1. Cycle-to-cycle correlations

	$\Phi_r(n)$ for run 1 (diffusion-dominated)			$\Phi_r(n)$ for run 2 (advection-dominated)		
		$r_{\rm s}$	$r_{\rm p}$		$r_{\rm s}$	$r_{\rm p}$
$\Phi_{\rm tor}(n)$	0.185	99.8%	*0.287*	0.653	100.0%	*0.778*
$\Phi_{\rm tor}(n+1)$	0.737	100.0%	*0.706*	0.805	100.0%	*0.851*
$\Phi_{\rm tor}(n+2)$	-0.040	49.1%	*0.028*	0.356	100.0%	*0.546*
$\Phi_{\rm tor}(n+3)$	0.195	99.9%	*0.202*	0.237	100.0%	*0.417*
$\Phi_{\rm tor}(n+4)$	0.036	44.5%	*0.056*	0.183	99.8%	*0.357*
$\Phi_{\rm tor}(n+5)$	0.107	92.3%	*0.073*	0.214	100.0%	*0.316*

Note. — Correlation coefficients and significance levels for peak surface radial flux Φ_r versus peak toroidal flux $\Phi_{\rm tor}$ for 275 cycles from stochastically forced dynamo simulations.